

Surface-Mediated Charge Transfer of Photogenerated Carriers in Diamond

Arsène Chemin, Igal Levine, Marin Rusu, Rémi Vaujour, Peter Knittel, Philipp Reinke, Karsten Hinrichs, Thomas Unold, Thomas Dittrich, and Tristan Petit*

Solvated electrons are highly reductive chemical species whose chemical properties remain largely unknown. Diamond materials are proposed as a promising emitter of solvated electrons and visible light excitation would enable solar-driven CO₂ or N₂ reductions reactions in aqueous medium. But sub-bandgap excitation remains challenging. In this work, the role of surface states on diamond materials for charge separation and emission in both gaseous and aqueous environments from deep UV to visible light excitation is elucidated. Four different X-ray and UV-vis spectroscopy methods are applied to diamond materials with different surface termination, doping and crystallinity. Surface states are found to dominate sub-bandgap charge transfer. However, the surface charge separation is drastically reduced for boron-doped diamond due to a very high density of bulk defects. In a gaseous atmosphere, the oxidized diamond surface maintains a negative electron affinity, allowing charge emission, due to remaining hydrogenated and hydroxylated groups. In an aqueous electrolyte, a photocurrent for illumination down to 3.5 eV is observed for boron-doped nanostructured diamond, independent of the surface termination. This study opens new perspectives on photo-induced interfacial charge transfer processes from metal-free semiconductors such as diamonds.

1. Introduction

Surface states in the bandgap of semiconductors have a decisive influence on the performance of electronic and photoelectric devices. In conventional semiconductors such as silicon, the density of surface states can be drastically reduced by surface passivation, i.e., by creating new chemical bonds that move electronic trap states out of the bandgap deep into the valence band (VB) and/or conduction band (CB).^[1,2] Diamond is a semiconductor with an ultra-wide bandgap of 5.47 eV^[3] and, in contrast to silicon surfaces, surface termination with atoms such as H, O, N, and F leads to electronic states within the bandgap.^[4,5] Therefore, diamond surfaces have a density of electronic states directly correlated to the surface termination that can be excited with light. This particularity opens great opportunities for achieving photoexcitation of charges at defined energies below the diamond bandgap by controlling the

surface termination. Sub-bandgap states can be further engineered by doping (e.g., N, P, and B),^[6] and nanostructuring the surface^[7–10] or using nanoparticles,^[11] offering higher surface area.


Charge transfer of photogenerated carriers in diamond drives many applications in electronics,^[12] brain implants,^[13–16] energy conversion,^[17,18] quantum sensing and computing,^[19] and (photo)electrochemistry.^[20–22] These applications rely on charge transfers such as photoexcitation and photoemission in vacuum, gas or aqueous electrolyte. For instance, diamond electrodes were shown to produce photocurrents induced by the excitation in the UV and the visible range.^[15,23–27] In particular, H-terminated boron-doped diamond combines the chemical stability of diamond and a high conductivity induced by doping with a negative electron affinity (EA) of the surface^[28] enabling the emission of solvated electrons that can be used for photo-induced chemical reduction of nitrogen^[29] and carbon dioxide molecules.^[7,30] Recently, the emission of solvated electrons in water under both UV^[31] and visible light^[11] excitation has been demonstrated through transient absorption. However, H-terminated diamonds suffer from oxidation in air and water, which is thought to hinder their emission properties,^[29] as oxygen-terminated diamonds are known to have a positive EA in vacuum.^[28] Several hypotheses involving surface states and dopant-related transition levels

A. Chemin, I. Levine, M. Rusu, T. Unold, T. Dittrich, T. Petit
Helmholtz-Zentrum Berlin für Materialien und Energie GmbH
14109 Berlin, DE, Germany
E-mail: tristan.petit@helmholtz-berlin.de

R. Vaujour
École Normale Supérieure de Lyon
Lyon 69342, France

P. Knittel, P. Reinke
Fraunhofer-Institut für Angewandte Festkörperphysik Freiburg
79108 Freiburg, DE, Germany

K. Hinrichs
Leibniz-Institut für Analytische Wissenschaften–ISAS–e.V.
12489 Berlin, DE, Germany

 The ORCID identification number(s) for the author(s) of this article can be found under <https://doi.org/10.1002/smt.202300423>

© 2023 The Authors. Small Methods published by Wiley-VCH GmbH. This is an open access article under the terms of the Creative Commons Attribution License, which permits use, distribution and reproduction in any medium, provided the original work is properly cited.

DOI: 10.1002/smt.202300423

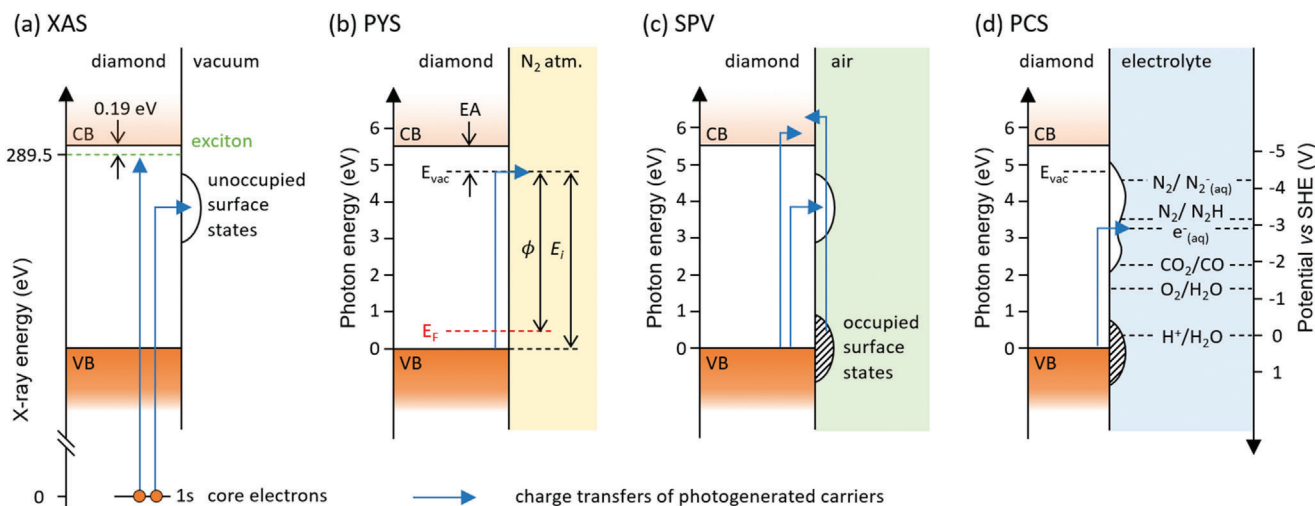


Figure 1. Schematic of charge transfer processes across a diamond surface detected by a) X-ray absorption spectroscopy, b) photoelectron yield spectroscopy, and c) surface photovoltage spectroscopy, and d) photocurrent spectroscopy.

have been formulated to explain low-threshold electron emission in vacuum^[32] and in water.^[14] Yet, a direct correlation between material properties and the light excitation, charge separation, and emission pathways is still lacking. Surface and defect states are often non-emissive and difficult to characterize by standard photoluminescence measurements, especially in the broad energetic range corresponding to the diamond bandgap. However, light-induced transitions from surface states into ultra-high vacuum, gas or electrolyte can be probed using photoelectric measurements.

In this work, four spectroscopy methods were combined to elucidate the role of surface states on the charge transfer of photogenerated carriers in diamond (**Figure 1**): X-ray absorption spectroscopy (XAS), photoelectron yield spectroscopy (PYS), surface photovoltage spectroscopy (SPV) and photocurrent spectroscopy (PCS). Synchrotron-based XAS uses X-rays to excite resonantly the transitions from the C 1s core electrons of diamond to unoccupied surface states, as shown in Figure 1a. This technique, which is element specific and highly surface sensitive,^[33] allows a precise characterization of the surface termination of the diamond.^[34,35] PYS collects the photoelectrons emitted from the surface in a nitrogen atmosphere upon UV–vis light absorption as shown in Figure 1b.^[36] The EA of the surface is derived from the emission onset according to the surface termination given by XAS. SPV probes the separation of charge carriers upon excitation in air,^[37,38] as shown in Figure 1c. The energy of these excitations is directly correlated with the energy levels of the unoccupied surface states provided by XAS and the emission of electrons given by PYS. Finally, PCS probes the emission of charges in an aqueous electrolyte upon monochromatic photoexcitation (Figure 1d). The diamond is used as the working electrode (WE) in a photoelectrochemical cell. PCS provides information on the effect of the electrolyte and is particularly relevant for practical (photo)electrocatalytic applications. When the quantum efficiency is computed, PCS is also referred as Incident Photon to Current Efficiency (IPCE).^[39] The diamond materials properties affecting photoexcitation and charge transfer processes are investigated by comparing diamond materials with different sur-

face terminations, doping, and surface nanostructuring. More precisely, nanostructured boron-doped diamonds, referred to as diamond black (DB),^[7] and (100) single crystal diamonds (SC) are compared. The intrinsic SC provides a well-defined system, while the DB is more relevant for practical applications. DB are produced from a 5 μm thick boron doped diamond ($\approx 10^{21} \text{ cm}^{-3}$) films grown by CVD on a silicon wafer. The film is then etched in an oxygen plasma with a mask of nickel nanoparticle leading to coral-like structure with the diamond grains still being distinguishable. The nanopillars obtained are hundreds of nanometres high and have a diameter of only few tens of nanometres. More details can be found elsewhere.^[7] DB offers an increased effective surface area, and its synthesis can be upscaled. Surface oxidation and its influence on charge transfer and emission have been studied by comparing H-terminated surfaces, referred to as H-SC and H-DB, with oxidized surfaces, referred to as O-SC and O-DB. After presenting the results obtained by each method, the correlative analysis of these diamond materials with the four complementary methods enables the drawing of a unified picture of the role of surface states on charge transfer processes at the diamond-air and diamond-water interfaces.

2. Results

2.1. Unoccupied Electronic States Related to Diamond Surface Termination

Figure 2 shows the X-ray absorption spectra at the C K-edge of the different diamond samples. The characteristic diamond features, including a large absorption above 289.5 eV due to the excitation of the core C 1s electrons to the CB of the diamond and a dip at 302.5 eV corresponding to a second absolute gap in the diamond band structure^[40] are observed for all samples. The sharp peak at 289.3 eV associated with transitions to the core exciton, which can be used to determine the CB minimum of the diamond by adding the energy of the core exciton measured elsewhere ($\approx 0.19 \text{ eV}$),^[41] as schematized in the Figure 1a. This core exciton is almost not observed on the DBs, especially on the O-DB, because the

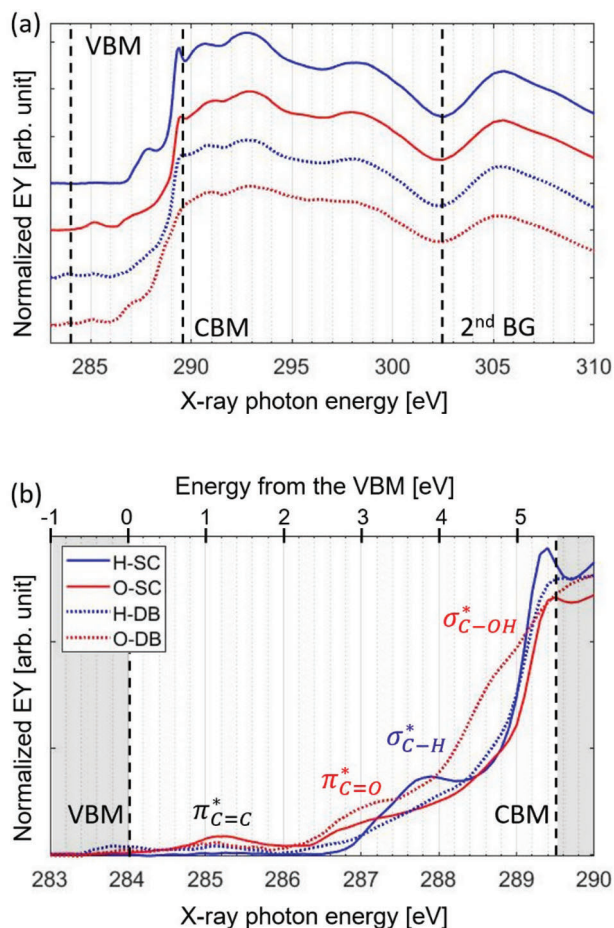


Figure 2. X-ray absorption spectra measured by electron yield (EY) at the C K-edge a) for a hydrogenated and oxidized diamond single crystal (H-SC and O-SC, solid blue and red lines, respectively) and for hydrogenated and oxidized diamond black (H-DB and O-DB, dashed blue and red lines, respectively). Spectra are normalized to their maximum and shifted for clarity. The intra-bandgap unoccupied states are highlighted in (b). The upper energy scale is referenced to the VB maximum (VBM), which is 5.47 eV below the CB minimum (CBM). The CB minimum is determined by the position of the core exciton (289.2 eV) \approx 0.19 eV below it.

surface crystal structure is strongly distorted by the nanostructuring and oxidation. The absorption features seen below are due to the excitation of C 1s electrons to unoccupied surface states with energies that lie within the diamond bandgap (see Figure 1a). The absorption at 285.2 eV is attributed to the C(1s) \rightarrow $\pi_{C=C}^*$ transitions from sp^2 carbon bonds found in surface defects^[4,42] induced by oxidation or nanostructuring of the surface.^[43] The absorption at 286.5 eV is attributed to C(1s) \rightarrow $\pi_{C=O}^*$ transitions from carbonyl groups.^[44] The signal at 287.8 eV was previously assigned to the C(1s) \rightarrow σ^* transition of carbon atoms bonded to hydrogen atoms.^[45] Finally, the shoulder at 288.7 eV is related to carbon atoms bonded to hydroxyl group.^[46]

Figure 2b compares the intensity of the pre-edge features. The H-SC surface shows only C–H surface groups, almost no sp^2 carbon bonds and no oxygen-containing surface groups as confirmed by the O K-edge XAS (Figure S1, Supporting Information) and XPS at the C 1s and O 1s (Figure S2 and S3, Supporting

Information). In contrast, the O-SC has a stronger sp^2 carbon signal and clear oxygenated groups, which consists of both carbonyl and hydroxyl groups. Despite the chemical oxidation of the surface, C–H groups are partially preserved, as confirmed by IR measurements (see Figure S4, Supporting Information). Exposure of the H-SC surface to water and UV leads to a similar oxidation of the surface with a larger proportion of hydroxyl groups compared to carbonyl groups (see Figure S5, Supporting Information), as previously reported on nanodiamonds.^[47] The H-DB shows some sp^2 carbon content from defects induced by surface nanostructuring and/or grain boundaries. A strong contribution from hydrogenated groups (\approx 25%) and some minor ones from hydroxyl (\approx 3.5%) and carbonyl groups (\approx 5%) are also detected (see Figure S3 and Table S2, Supporting Information). The O-DB sample, on the other hand, shows mainly hydroxyl and carbonyl groups (\approx 7.8% for both). Compared to the O-SC sample, more hydroxyl groups are observed. Most intriguingly, the DB surface also absorbs \approx 284 eV, possibly assigned to carbon dimers induced by surface reconstruction,^[48] boron-related defects, or silicon-related defects since the DBs are grown on silicon wafers.

The energy of the surface states in the diamond sub-bandgap region can be extracted by estimating the position of the CB minimum from the core exciton. Their energy relative to the diamond VB maximum, considering a bandgap of 5.47 eV, is given by the upper scale in Figure 2b. The position corresponds to the VB onset reported for X-ray emission spectroscopy at 284.1 eV.^[43]

2.2. Electron Affinity in Nitrogen Atmosphere

The surface termination of diamond has a direct influence on the EA of the surface due to the dipoles created by the terminating chemical bonds, which in turn affects the emission of electrons. For example, H-terminated diamonds are known to have a strongly negative EA in vacuum, reaching up to -1.3 eV.^[28,49] On the other hand, oxygen-terminated diamonds often have a positive EA due to the strong electronegativity of the carbonyl group.^[28] The EA of diamond surfaces can be derived from the measured onset of the photoelectron yield.^[50,51] In the case of diamond, excitation occurs from VB electrons, as shown in Figure 1b. Near the emission onset, the photoelectron yield $Y(h\nu)$ can be approximated by: $Y(h\nu) \propto (h\nu - E_i)^3$, where $h\nu$ is the energy of the incident photon and E_i the ionization energy of the surface.^[52] The ionization energy of the surface is thus determined by a linear fit of the $Y(h\nu)^{1/3}$ onset as shown by the thin solid lines in Figure 3 and summarized in Table 1. The EA is determined as the difference between the ionization energy and the bandgap (5.47 eV).

As expected, H-SC has a very strong negative EA of -0.82 eV. The chemically oxidized sample O-SC also has a negative EA, albeit smaller, of -0.45 eV, which is related to residual C–H groups and the presence of hydroxyl groups, clearly observed by XAS and IR (see Figure S1, Supporting Information). Compared to H-SC (O-SC), H-DB (O-DB) has a reduced negative EA of -0.36 eV (-0.17 eV), probably due to an increased number of defects as the doping state has little effect on PYS (see Figure S6, Supporting Information). Nevertheless, all these measurements show that even after partial oxidation of the diamond surface, the presence of hydroxyl groups and remnant CH groups is sufficient to

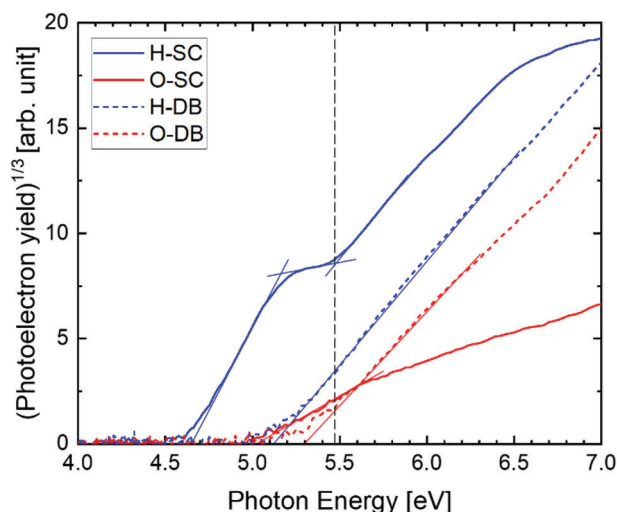


Figure 3. Photoemission spectra $Y(h\nu)^{1/3}$ for H-SC (solid blue), H-DB (dashed blue), O-SC (solid red), and O-DB (dashed red). The vertical dashed line corresponds to the bandgap of the diamond at 5.47 eV, while the thin solid lines represent the linear fits.

maintain a negative EA, in agreement with previous work performed in vacuum.^[53] This is highly relevant for practical applications in aqueous electrolytes as we will discuss in Section 3.5.^[7] In addition, H-SC shows an emission decrease at 5.12 eV that is not observed in the other samples. Correlated with SPV and PCS measurements, this dip is associated with the excitation of a strongly bound exciton, which will be discussed in more detail in the discussion.

In parallel, the work function (ϕ) of the surface is measured using the Kelvin probe technique. The position of the Fermi level (E_F) relative to the VB maximum (E_{VBM}) at the surface can be determined by $E_F - E_{VBM} = \phi - E_i$. These measurements are summarized in Table 1. For boron-doped DB, the Fermi level is measured to be close to the VB maximum as expected and observed since the boron acceptor levels are 0.36 eV above the VB maximum.^[54,55] More surprisingly, the Fermi level of the intrinsic SC also appears close to the VB maximum, either due to residual impurities in the crystal or strong surface band bending. The work function measured on O-SC gives $E_F - E_{VBM} > 0$ which means that the Fermi level is below the VB maximum. This can be explained by either an upward surface band bending, or a negative surface dipole associated with the O-surface termination, or both.

Table 1. Surface work function ϕ measured by Kelvin probe, ionization energy E_i determined by PYS, electron affinity EA, and position of the Fermi level relative to the VB maximum.

Sample	ϕ (± 0.04 eV)	E_i (± 0.03 eV)	EA (± 0.04 eV) ^{a)}	$E_F - E_{VBM}$ (± 0.04 eV) ^{b)}
H-SC	4.51	4.65	-0.82	-0.14
O-SC	5.12	5.02	-0.45	0.1
H-DB	5.08	5.11	-0.36	-0.03
O-DB	4.89	5.30	-0.17	-0.36

^{a)} EA = $E_i - E_g$ with $E_g = 4.7$ eV the diamond bandgap; ^{b)} $E_F - E_{VBM} = \phi - E_i$

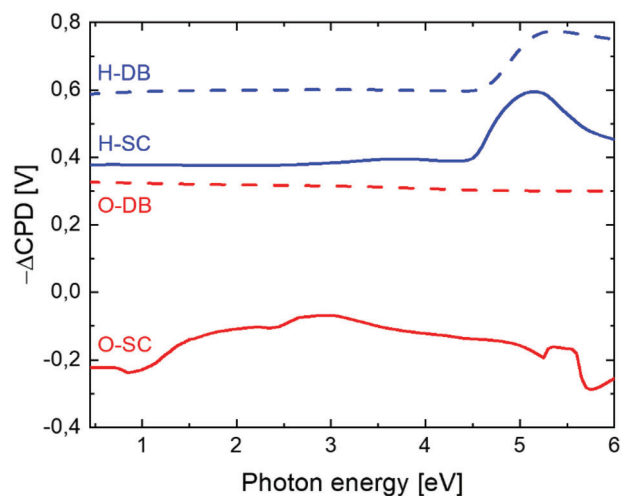


Figure 4. SPV spectra of H-SC (blue solid line), O-SC (red solid line), H-DB (blue dashed line), and O-DB (red dashed line), measured by the Kelvin probe technique.

2.3. Separation of Photogenerated Charge Carriers

SPV measurements characterize the separation of photogenerated charge carriers in the sample. Following the absorption of photons, electron-hole pairs are generated in the sample and may separate due to asymmetric trapping at surface states, drift in built-in electric fields, etc. By measuring the contact potential difference ($-\Delta\text{CPD}$) between the sample and a reference electrode in the dark and under light illumination, it is possible to define $-\Delta\text{CPD} = \text{CPD}_{\text{light}} - \text{CPD}_{\text{dark}}$ (convention: the SPV is defined as the negative change of the ΔCPD) which characterizes charge separation in the sample. **Figure 4** shows the spectra of $-\Delta\text{CPD}$ measured on the samples H-SC, O-SC, H-DB, and O-DB. The spectra were measured starting from the lowest photon energy. The values of $-\Delta\text{CPD}$ start at +0.38, -0.22, +0.59, and +0.33 V for H-SC, O-SC, H-DB, and O-DB, respectively. The oxidized diamond surfaces are more negative compared to the hydrogenated diamond surfaces because of the additional negative surface dipole due to the oxygen bonds. This is also reflected in the different EAs in the PYS measurements. The difference is smaller for the DB samples because the very high density of defect states mitigates the influence of surface oxidation on the initial contact potential difference. In addition, the doping increases the positive surface polarization, which is also observed on boron-doped SC (see Figure S7, Supporting Information).

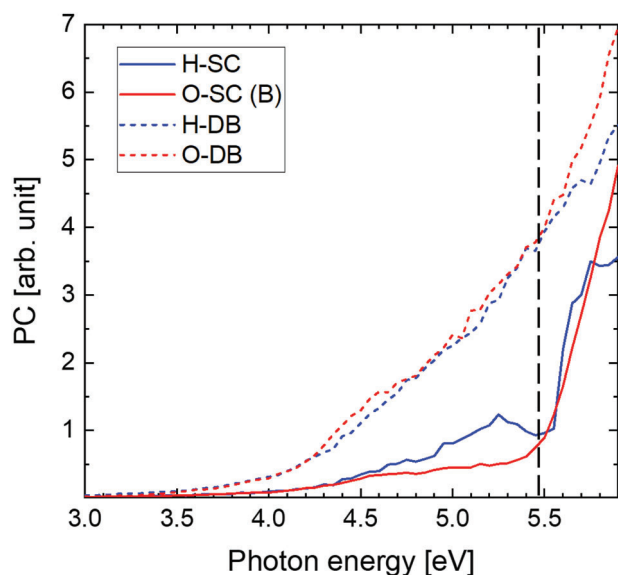


Figure 5. Photocurrent spectra of H-SC (solid blue line), O-SC (B) (solid red line), H-DB (blue dashed line), and O-DB (red dashed line). The potential of the WE (diamond) is set to -0.3 V versus Ag/AgCl in 3 M KCl.

Transition energies in $-\Delta$ CPD spectra are determined by the conventional approach. A change in the slope of $-\Delta$ CPD toward more positive (negative) corresponds to the onset of a transition leading to a net separation of electrons (holes) toward the bulk or of holes (electrons) toward the surface. Linear fits near the transitions and second derivative help determine when the slope of $-\Delta$ CPD changes giving a good approximation of the transition energies as shown in Figure 6 (blue curves) in Section 5. By far the largest number of features was observed in the spectrum of $-\Delta$ CPD for O-SC. The number of transitions observed and their amplitude is much more important for the SCs than for the DBs because doping increases charge mobility and recombination. The same has been observed on boron-doped SC (see Figure S7, Supporting Information). The appearance of additional transitions for O-SC compared to H-SC can be interpreted as the appearance of transitions involving surface states, since surface oxidation is unlikely to affect bulk states (such as defects, etc.). The origin of the transition will be further discussed in the next section by combining the four different measurement techniques.

2.4. Photo-Induced Charge Transfer into an Aqueous Electrolyte

Charge transfer into an aqueous electrolyte is characterized by the photocurrent resulting of the monochromatic illumination of the diamond samples as shown in Figure 5. For O-SC, a boron-doped SC, referred as O-SC (B), was used because the resistance of the oxidized intrinsic SC was too high for photocurrent measurements. A positive photocurrent corresponds to the transfer of negative charges from the diamond to the electrolyte. As mentioned above, negative charges can be transferred to the electrolyte by the emission of solvated electrons.^[11] Although no redox reaction is observed in the CV curves at the working potential (see Figure S8, Supporting Information), even under illumina-

tion, a photo-induced reaction of the adsorbate or surface group cannot be excluded.

Above the bandgap, a strong photocurrent increase observed for the SC is attributed to band-to-band excitation, suggesting direct emission of electrons from the CB into the electrolyte.^[29] At this stage, we do not have further information about the solvation state of the emitted electron or possible chemical reaction with dissolved species in the electrolyte. In any case, an electron transfer leading to a strong photo-induced current is clearly evidenced. For the DB, no clear increase is observed, possibly due to the strong sub-bandgap photocurrent. The four samples show significant photocurrent for sub-bandgap excitation. In contrast to PYS in nitrogen atmosphere, the photocurrent starts for excitation down to 3.5 eV. The sub-bandgap photocurrent of DB is much larger than that of SC, which can be attributed to the increased surface area due to nanostructuring, resulting in a higher density of surface states and an increased diamond-water interface. The photocurrent decrease observed for H-SC is correlated with the decrease observed in PYS and is also attributed to the excitation of strongly bounded excitons, which will be discussed in more detail below.

3. Discussion

3.1. Correlative Spectroscopy of Photoexcitation in Diamond

A comparison of the spectra obtained from the different techniques is shown on a unified scale in Figure 6. The X-ray absorption features related to resonance exciton absorption, 0.19 eV below the CB minimum, provides a reference to position the energy of the unoccupied surface states within the bandgap. The position of the unoccupied surface states can then be correlated to the SPV transition to identify their nature. Transitions are labeled with letters A through H depending on their identified origins, and with a number index if several transitions with the same origin are observed at different energies (Table 2). Unidentified transitions are marked with an asterisk. In correlation with PYS and PCS, these transitions provide new insights into the role of surface states in the charge transfer of photogenerated carriers. In the following, we discuss the different types of transitions based on their origin.

3.2. Phonon-Assisted Excitons

First, the excitonic transitions that are not directly related to surface states are discussed. The transitions G (see Figure 6 and Table 2) are related to transitions of VB electrons to an indirect exciton state in the bulk of the diamond, which is associated with the absorption or the emission of phonons. Similar to the exciton observed in XAS, it corresponds to an electron excited in the CB that is bound to the hole. But here, the hole is located in the VB and not in the C 1s energy level as for XAS. Exciton-related transitions are not observed on the DB due to the fast recombination or lack of phonon coupling due to defects and surface nanostructures.

Figure 7 shows a close-up measurement with the first and second derivative of $-\Delta$ CPD. The energies of the transitions G_1 and

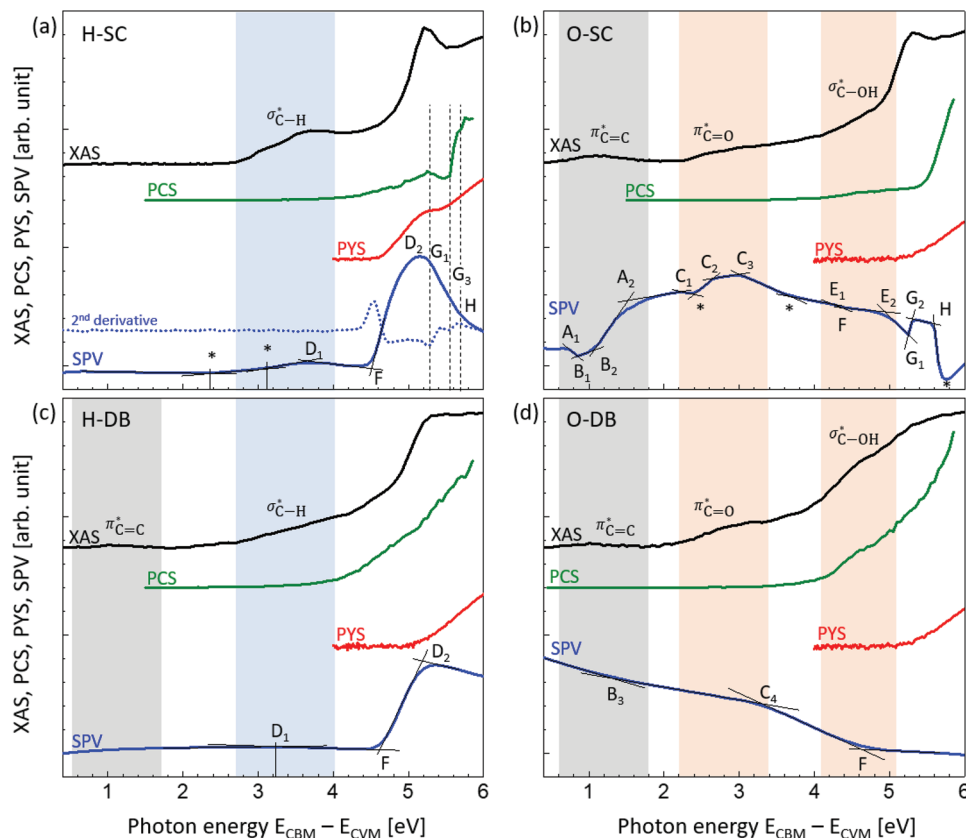


Figure 6. Comparison of XAS (black), PYS (red), PCS (green), and SPV (blue) for a) H-SC, b) O-SC, c) H-DB, and d) O-DB. The X-ray photon energy of the XAS is shifted to match the position of the CB minimum. Energy regions corresponding to unoccupied surface states determined by XAS are indicated by the colored area. Transitions identified by SPV are summarized in Table 2.

Table 2. Transition energies in samples H-SC, O-SC, H-DB, and O-DB, and assignments from the combination of XAS and SPV.

Transition label	Surface charge ^{a)}	Transition energy [eV]				Transition origin
		H-SC	O-SC	H-DB	O-DB	
A ₁	–		0.7			VB → π _{C=C} [*]
A ₂	–		1.35–1.85			VB → π _{C=C} [*]
B ₁	+		0.85			C–OH → CB
B ₂	+		1.05			C–OH → CB
B ₃	+				1.35	C–OH → CB
C ₁	–		2.25			VB → π _{C=O} [*]
C ₂	–		2.65			VB → π _{C=O} [*]
C ₃	–		3.0			VB → π _{C=O} [*]
C ₄	–				3.3	VB → π _{C=O} [*]
D ₁	–	3.65		3.25		VB → σ _{C–H} [*]
D ₂	–	4.80–5.20		5.20		VB → σ _{C–H} [*]
E ₁	–		4.2			VB → σ _{C–OH} [*]
E ₂	–		4.8–5.0			VB → σ _{C–OH} [*]
F	+	4.35–4.65	4.4	4.5–4.7	4.45–4.8	C–H → CB
G ₁	– / +	5.27	5.27			E _g – E _x – hν _{LO/LA}
G ₂	–		5.32			E _g – E _x – hν _{TA}
G ₃	–	5.53				E _g – E _x + hν _{LO/LA}
H	+ / –	5.6	5.6			E _g + hν _{TO}

^{a)} The surface charge refers to the sign of the charge preferentially moving toward the surface of the sample and is determined by the change in the – ΔCPD slope.

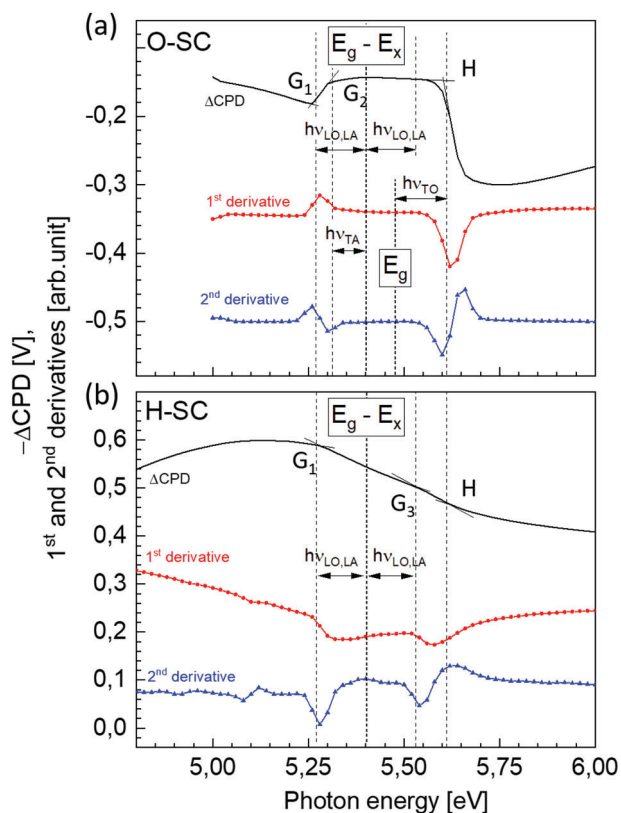


Figure 7. SPV (black) and its first (red) and second derivatives (blue) for a) H-SC and b) O-SC in the bandgap region. Vertical dashed lines represent relevant transition energies. Transitions identified by SPV are indicated by letters corresponding to Table 2.

G_3 are $E_g - E_x \pm hv_{LO/LA}$ where E_g , E_x , and $hv_{LO/LA}$ are the energies of the bandgap (5.47 eV), of the indirect exciton (0.07 eV) and of the longitudinal optical and acoustic phonons (0.132 eV), respectively.^[3] The energies of the transition G_2 is $E_g - E_x - hv_{TA}$, where hv_{TA} is the energy of the transversal acoustic phonon (0.083).^[3] These phonon-assisted transitions and excitons have already been observed by the SPV technique.^[37,38] The surface termination seems to influence the phonon coupling as G_2 is observed on O-SC only and G_3 on H-SC only. An exciton, being a bound state between an electron and a hole, can be measured by SPV only if it dissociates before recombining so that the charges can move apart. G_1 and G_2 are particularly visible for O-SC (see Figure 7a), indicating significant exciton dissociation with preferential hole and electron trapping in surface states respectively. In contrast, G_1 and G_3 are much weaker for H-SC, but still noticeable in the second derivative of $-\Delta\text{CPD}$ (see Figure 7b, blue curve), indicating little dissociation of the exciton prior to recombination. This time, the dissociation of both excitons leads preferentially to electrons trapped at the surface. The surface termination seems to strongly influence the exciton dissociation process.

The strongly bound exciton state observed on H-SC, prevents the emission of charges as it is hard to dissociate. The excitation G_1 at 5.27 eV correlates very well with the decrease in charge emission observed in PYS and PCS (see Figure 6a). The same process could happen for the transition G_3 , which could explain

why the photocurrent increases strongly only after 5.6 eV and not after 5.47 eV, but the overlap with the excitation of free electrons in the CB makes it more difficult to discuss. Note that this effect disappears when the surface is partially oxidized, as shown in the PYS measurements made on the same diamond sample after exposure to water and UV (see Figure S9, Supporting Information).

3.3. Excitation above the Bandgap

The charge displacement after excitation above the bandgap energy is not obvious in the SPV measurements because it starts in the same energy range as the excitons mentioned above. In SC, the transition H can be observed at the energy $E_g + hv_{TO}$ where E_g , and hv_{TO} are the energies of the bandgap (5.47 eV), and the transverse optical phonons (0.143 eV), respectively.^[3] This transition is very weak for H-SC and seems to be associated with electrons preferentially moving to the crystal bulk while H is very strong on O-SC and associated with electrons preferentially moving to the crystal surface. This may indicate a different band bending direction between the two surface terminations, but further study is needed. To investigate further the charge separation for excitation above the bandgap, transient SPV has been acquired (Figure S10, Supporting Information). Transient SPV allows the monitoring of the surface polarization as a function of time after the laser pulse excitation for photon energies between 5.6 and 5.9 eV, hence above exciton and phonons related transitions. The transient SPV confirms that free electrons excited to CB preferentially go toward the surface for all the samples. This is coherent with the electron transfer to the gas atmosphere or electrolyte clearly observed at these energies by PYS and PCS, respectively. As in PYS, such excitation can lead to electron emission due to the negative EA of the surfaces. In SPV, however, no bias potentials are used, leading to an accumulation of negative charges at the surface of the crystal.

3.4. Sub-Bandgap Charge Transfer

Transitions from occupied surface states in the bandgap to the CB are identified for excitation energies below 5.47 eV. For such transitions, the charge separation leads to a positive polarization of the surface, characterized by SPV (see Table 2). This is the case of the transitions B and F, corresponding to the excitation of occupied C—OH and C—H states, respectively. Indeed, the transitions B_1 and B_2 , observed on O-SC at 0.85 and 1.05 eV (see Figure 6b), and the transition B_3 , observed on O-DB at 1.35 eV (see Figure 6d), are not observed on H-SC and H-DB. Their energies are close to the difference between the unoccupied σ_{C-OH}^* state and the CB minimum, so they probably arise from the excitation of these partially occupied surface states. The transition F generates the strongest SPV signals, observed for samples H-SC and H-DB ≈ 4.5 eV, and corresponding to a variation of 0.206 V and 0.177 V, respectively (see Figure 6a,b). The similar onset energies and the similar high positive SPV signals provide evidence that the charge separation is caused by charge transfer across the diamond surface and that the bulk diamond has negligible influence on the charge separation. Transition F is also observed on the oxidized samples with a much weaker intensity, which is

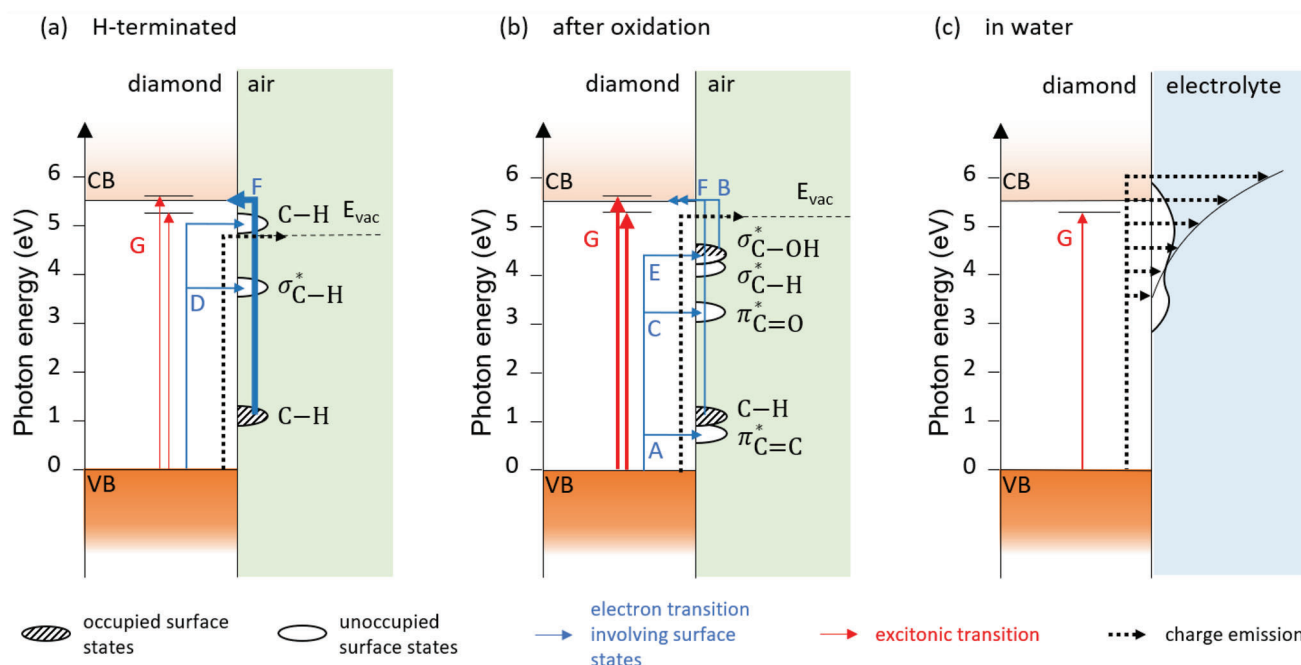


Figure 8. Charge transfer processes across a H-terminated diamond surface mediated by surface states in air a) before and b) after oxidation and in c) water derived from the combination of XAS, PYS, PCS, and SPV. The position of the vacuum level is determined by the onset of the PYS emission. Unoccupied surface states are determined by XAS and shown in white. Occupied states are derived from SPV measurements and shown with hatches. In water (c), the unoccupied surface states have not been measured and are shown schematically.

consistent with the remaining CH groups observed by XAS. Although XAS cannot access occupied states, recent calculations on (100) boron-doped diamonds predict the presence of such occupied surface states within the diamond bandgap. These surface states have energies between 0.7 and 1.7 eV below the CB minimum for hydroxylated surfaces, and up to 2.8 eV below the CB minimum for hydrogenated surfaces.^[5] The transitions B and F identified here are consistent with both the energy position of these states and their origin.

In contrast to the previous transitions, A, C, D, and E lead to negative surface polarization (see Table 2) and can be attributed to the excitation of VB electrons to unoccupied surface states. These states are characterized by XAS and the energy correlation on the Figure 6 (see colored energy ranges) enables to determine the origin of the transitions. Transitions A, from 0.7 eV to 1.85 eV, correspond to the excitation of the $\pi_{C=C}^*$ unoccupied states of sp^2 carbon and are superimposed with the transitions B (see Figure 6b). These transitions are only observed on O-SC, which correlates well with the small amount of sp^2 carbon defects detected on H-SC by XAS. More surprisingly, they are not observed on DB despite a large amount of sp^2 carbon defects. In DB, the boron doping increases the recombination rate of the charges so that the SPV cannot detect the charge separation, which is also observed on boron-doped SC (see Figure S7, Supporting Information). Transitions C, observed on O-SC at 2.25, 2.65, and 3.0 eV (see Figure 6b), and O-DB at 3.3 eV (see Figure 6d), correspond to the excitation of unoccupied $\sigma_{C=O}^*$ states. The transition D₁, clearly observed at 3.65 eV on H-SC and 3.25 eV on H-DB, is attributed to the excitation of unoccupied σ_{C-H}^* states (see Figure 6a,c). The transition D₂, observed \approx 5 eV on these samples,

is very similar and likely due to the excitation of VB electrons to C–H related surface states. However, it is difficult to correlate this transition with XAS because of the predominance of the carbon absorption edge. The observed shifts and intensity variations between both samples are attributed to surface defects and different C–H boundary environments on H-DB, as evidenced by broader XAS features. Finally, transitions E₁ and E₂, only observed on O-SC between 4.2 and 5.0 eV, corresponds to the excitation of unoccupied σ_{C-OH}^* states (see Figure 6b). They are not observed on O-DB nor doped SC (see Figure S7, Supporting Information), for the same reason as the transitions A.

3.5. Role of Surface Termination on Charge Emission from Diamond Materials

The direct correlation between the different spectroscopy techniques allows a description of the charge emission for the different diamond surface terminations. H-terminated diamonds are known to be good electron-emitters due to the negative EA of their surface. However, they suffer from oxidation in air and water, especially when exposed to UV light, which is thought to reduce their ability to emit electrons in liquid.^[29] To discuss this issue, the different charge transfer processes identified in this study are summarized in **Figure 8** for an H-terminated diamond surface exposed to air before a) and after oxidation b) and exposed to an aqueous electrolyte c).

Surface characterization by XAS revealed that chemical oxidation of the diamond results in a significant amount of carbonyl groups, hydroxyl groups, and sp^2 carbon defects, but many C–H

groups are retained. Thus, the surface EA in air, as measured by PYS, is reduced by oxidation, but remains negative (Figure 8b). The emission of electrons in air is strongly dominated by direct ionization (dashed black arrows in Figure 8a,b). The onset is defined only by the negative EA. Although the dipoles created by the surface termination influence the negative EA of the surface and the emission onset, the excitation of the surface state is not directly involved in the emission.

SPV revealed that many surface states within the diamond bandgap are photoactive, especially on the oxidized surface, which shows different types of chemical bonds (blue arrows in Figure 8a,b). VB electrons can be excited to unoccupied surface states, well characterized by XAS, and electrons from occupied surface states, predicted by calculations,^[5] can be excited to the CB. Although characterized in air, the photoactivity of these surface states is promising for visible light photoelectrochemical applications. It should be noted that the exact nature of the unoccupied electronic states may vary upon interaction with the electrolyte. In water, XAS performed on nanodiamonds shows a large number of new vacancies that could be involved in charge transfer with the liquid.^[35]

In an aqueous electrolyte, the onset of the photocurrent at 3.5 eV seems to correlate with the transition D_1 (excitation of σ_{C-H}^* states). Such a low onset is consistent with the emission of solvated electrons and the photocurrent observed for excitation below the diamond bandgap.^[11,13,56] Furthermore, the total photocurrent seems to be largely independent of the surface termination, especially for DBs. This may explain the good photocatalytic behavior reported for both H-DB and O-DB,^[57] which would not be expected from EA measurements alone. Nanostructured materials such as DB could help to overcome the strong decrease in solvated electron emission observed on oxidized surfaces.^[29] A bound exciton state observed on the H-SC can limit the charge emission in gas and in liquid, as demonstrated by the combination of SPV, PYS, and PCS. Fortunately, this effect disappears for boron-doped diamonds and as soon as the surface is partially oxidized and does not hinder the photoelectrocatalytic application.

The implications of observing different charge emission after photoexcitation in gaseous and liquid atmospheres highlight the need for in situ characterizations, directly in the liquid. The electronic interaction with a liquid environment cannot always be predicted by vacuum or ambient air characterizations. The nature of the charge transfer at the diamond-water interface remains to be studied in more detail, but it appears clear that it differs from known electron emission mechanisms in vacuum or in air. X-ray spectroscopy at the carbon K-edge in liquid is experimentally very challenging due to the necessity to perform soft X-ray experiments in vacuum. Measurement in water have been achieved on nanodiamonds colloidal dispersions flown in a microjet and show a great increase of unoccupied states induced by charge transfers.^[35] Such a technique cannot be transferred to diamond substrate, but one can expect similar effects to take place. Sub-bandgap charge emission is highly relevant for visible light-driven CO_2 or N_2 photoelectrochemical reduction reactions and should be further investigated. Other strategies, such as functionalization of diamond surfaces with dyes, are being developed for this purpose,^[20,57] and could be studied in the same way to elucidate the excitation processes involved in their photocatalytic performance.

4. Conclusion

The combination of XAS, PYS, SPV, and PCS allows a direct correlation between charge separation processes and the surface properties of diamond. Charge separation in diamond in air was investigated by SPV and appears dominated by the surface states for photoexcitation below the bandgap. The oxidation of the surface provides a large variety of unoccupied surface states ($C\equiv C$, $C=O$, $C-H$, and $C-OH$) characterized by XAS having an energy within the bandgap of the diamond. The correlation of all measurements shows the excitation of VB electrons to discrete unoccupied surface states in intrinsic diamond crystals. Comparison of the SPV signal from hydrogenated and oxidized surfaces also characterizes the excitation of occupied $C-H$ and $C-OH$ surface states, in agreement with recent calculations. In boron-doped diamonds, a very high density of bulk defect states hinders the experimental observation of these excitations due to fast recombination. Only the excitation associated with $C-H$ surface states at ≈ 4.5 eV and ≈ 5 eV remains significant. However, this does not limit the charge emission from boron-doped diamonds in both gaseous and aqueous environments.

In gaseous environment, the emission of electrons characterized by PYS is driven by direct ionization and the EA of the surface. Oxidation of the surface reduces the EA which remains negative because of persistent $C-H$ and $C-OH$ surface bonds. Consequently, the onset of the emission occurs for larger energy of photoexcitation (≈ 5 eV against 4.5 eV for clean H-SC). In aqueous electrolytes, a photocurrent is observed for photoexcitation at energy as low as 3.5 eV for boron-doped nanostructured diamond. The previous observation in gaseous environment enlightens the potential role of the surface states in the charge separation and in the emission of solvated electron. Yet, no direct correlation with ex situ characterizations is observed and the photocurrent is largely independent of the surface termination. This set diamond as a unique material to explore the emission and fundamental properties of solvated electrons though in situ characterisation. Furthermore, surface oxidation of diamond is not prohibitive for photoelectrocatalytic reduction reactions, and the low energy onset opens new perspectives toward visible-light energy conversion.

5. Experimental Section

Samples: Single crystal (SC) diamonds have an oriented (100) surface. They were $3 \times 3 \text{ mm}^2 \times 300 \text{ }\mu\text{m}$ intrinsic diamonds consisting of a CVD substrate (optical grade, with ≈ 1 ppm of p1 Nitrogen) overgrown with a 15 μm ultrapure diamond layer (no detectable contamination, electronic grade). Boron-doped diamond single crystals (SC (B)) were used for complementary study of the boron doping effects (Figure S6 and S7 and S9, Supporting Information) and for the photocurrent measurements (see Figure 5). They were $3 \times 3 \text{ mm}^2 \times 250 \text{ }\mu\text{m}$ boron-doped HPHT substrates with ≈ 300 ppm ($5 \times 10^{19} \text{ cm}^{-3}$). In addition, diamond black nanostructured boron-doped diamond (DB) were prepared by ion etching of a polycrystalline boron-doped diamond wafer with an average of 5700 ppm (10^{21} cm^{-3}).^[7] One of each type was subjected to hydrogen plasma treatment, resulting in H-terminated surfaces (referred to as H-SC, H-SC (B), and H-DB, respectively). The other samples were artificially aged and partially oxidized by wet chemical treatment (referred to as O-SC, O-SC (B), and O-DB, respectively). Oxidation was performed in a mixture of sulfuric acid and nitric acid (ratio 3:1) for 1.5 h at elevated temperatures.

X-Ray Absorption Spectroscopy (XAS): X-ray absorption spectroscopy (XAS) was performed at the Russian-German beamline of the electron storage ring BESSY-II at Helmholtz-Zentrum Berlin (Germany) using an ultrahigh vacuum experimental station.^[58] The measurements were conducted in the electron yield (EY) mode, where the incident photon energy was swept and the emitted electrons from the sample were simultaneously recorded under a 150 V screening potential, which selects the electrons with high energy and increased the surface sensitivity of the technique. The beamline was optimized for NEXAFS spectroscopy in the VUV range, and carbon contamination from the beamline's optical elements was removed by oxygen plasma cleaning, resulting in a significant decrease of the carbon contamination signal. The spectra were normalized by the incident photon flux and between the pre-edge and post-edge regions, with no background correction needed. The energy resolution of the monochromator in the range of the C 1s (≈ 285 eV) X-ray absorption edges was ≈ 70 meV. The X-ray energy was calibrated against the energy positions of the first narrow peak of the C 1s absorption spectrum of highly ordered pyrolytic graphite (HOPG) (≈ 285.45 eV). X-ray photoelectron spectra (XPS), see Figure S2 and S3 (Supporting Information), were calibrated in accordance with the position of the reference highly ordered pyrolytic graphite (HOPG) peak (≈ 284.7 eV).

Photoelectron Yield Spectroscopy (PYS): PYS was performed in an ambient pressure environment of nitrogen gas using an SKP 5050-APS02 from KP Technology. The setup was placed in a Faraday cage to shield external electric fields and enable controlled illumination of the sample. The samples were contacted with carbon tape and mounted on a motorized 3-axis stage with a precision of less than 300 nm. The top counter electrode was a 2.0 mm diameter electrode with a gold-alloy coating. The tip-sample static distance was ≈ 1 mm. A bias voltage of 10 V was applied between the sample and the electrode to collect the charges. The sample was illuminated by a deuterium light source coupled with a grating monochromator, providing excitation from 3.4 to 7.6 eV. Measurements were conducted with a step of 1 nm and the photoemission threshold was determined with a resolution of 30 meV. The light was guided by a DUV optical fiber and focused on the sample with an elliptical spot of $\approx 3 \times 4$ mm². Unlike vacuum measurements, the electronic current was indirectly collected by the ionic current created by the ionization of the atmosphere due to the emission of electrons from the sample.^[36] The information depth (ID) in PYS measurements depends on the inelastic mean free paths (IMFPs) of the electrons excited from the elements comprised in the sample and was determined as: $ID = 3 \times IMFP$. For diamonds the theoretical value for IMFP extrapolated for low electron energies was 10 nm. Thus, the maximum ID in the PYS measurements was estimated of ≈ 30 nm.^[59]

Surface Photovoltage (SPV): SPV measurements were performed in the dc (Kelvin-probe) regime on a set-up with a perforated electrode ($\Delta\phi$ Besocke) and a charge amplifier (Elektronik Manufaktur Mahlsdorf) and a quartz prism monochromator (SPM2, Carl Zeiss Jena) for illumination (see references^[37,60] for details). Values of transition energies can be well-defined in the small signal case and if there was only one dominating mechanism of charge separation. However, SPV signals were usually not proportional to the photon flux and processes with opposite direction of charge separation can occur. Furthermore, baselines were not well-defined for spectral dependent SPV measurements in the dc (Kelvin-probe) regime due to slow charging and discharging processes and the measurement regime can influence the value of a transition energy. For these reasons, the spectra of $-\Delta CPD$ were not normalized to the photon flux and one needs to further consider the spectral features of the lamp.

Photocurrent Spectroscopy (PCS): The diamond samples were used as the working electrode (WE) in a spectroelectrochemical flow cell (SEC-3F, C3-Analysentechnik). The area of the working electrode was limited to 0.8 mm². The diamond samples were contacted with copper tape at the back of H-DB and O-DB samples (conductive) and on the top of H-SC. The surface conductivity of H-SC was high enough so that undoped diamond was used. For the O-SC sample, photocurrent measurements were performed on boron-doped diamond (O-SC (B)). The counter electrode (CE) was made of a stainless-steel tube with a surface of ≈ 75 mm². The potential on the WE was set versus an Ag|AgCl reference electrode by an SP-200 potentiostat from Biologic and recording the current. A positive

current corresponds to the flow of negative charge from the WE to the CE. All photocurrent measurements were carried out in an aqueous 3 M KCl electrolyte which was transparent up to photon energies of ≈ 5.9 eV. A laser driven light source (LDLS EQ-99X-CAL-S, Hamamatsu) with a home-made quartz prism monochromator (T. Dittrich, S. Fengler) was used for modulated illumination (modulation frequency 1.8 Hz) in the range of photon energies between 0.45 and 6.2 eV. The modulated photocurrent was measured with a lock-in amplifier (EG&G 5210). The corresponding photocurrent spectra were normalized to the light intensity. Some current-voltage characteristics were shown in Figure S8 (Supporting Information). A potential of -0.3 V versus Ag|AgCl was chosen for all photocurrent measurements. At this potential, photocurrent signals could be well detected, and redox reactions were avoided.

Supporting Information

Supporting Information is available from the Wiley Online Library or from the author.

Acknowledgements

This work was funded by a Freigeist Fellowship from the Volkswagen Foundation (n° 89592). I.L. and T.D. are grateful to BMWi for financial support (KK5085302DF0). This study was possible thanks to the technology developed by Dr. Steffen Fengler and Dr. Thomas Dittrich on SPV. The X-ray absorption spectroscopy was achieved at the BESSY II synchrotron on the HE-SMG beamline with the help of Dr. Maria Brzhezinskaya. Technical support by Ö. Savas is acknowledged. Funding was gratefully acknowledged: Application Lab for Infrared Ellipsometry via the Europäischer Fonds für regionale Entwicklung (EFRE, 1.8/13); Ministerium für Kultur und Wissenschaft des Landes Nordrhein-Westfalen; Die Regierende Bürgermeisterin von Berlin–Senatsverwaltung Wissenschaft, Gesundheit, Pflege und Gleichstellung; Bundesministerium für Bildung und Forschung.

Open access funding enabled and organized by Projekt DEAL.

Conflict of Interest

The authors declare no conflict of interest.

Data Availability Statement

The data that support the findings of this study are available from the corresponding author upon reasonable request.

Keywords

photoelectron yield spectroscopy, photocurrent spectroscopy, surface chemistry, surface photovoltage, X-ray absorption spectroscopy

Received: March 31, 2023
Revised: June 20, 2023
Published online: August 18, 2023

- [1] N. E. Grant, S. L. Pain, J. T. White, M. Walker, I. Prokes, J. D. Murphy, *ACS Appl Energy Mater* **2022**, *5*, 1542.
- [2] S. Rauscher, T. Dittrich, M. Aggour, J. Rappich, H. Flietner, H. J. Lewerenz, *Appl Phys Lett* **1995**, *66*, 3018.

- [3] C. D. Clark, P. J. Dean, P. V. Harris, *Proc. R. Soc. Lond. A* **1964**, 277, 312.
- [4] Z. Shpilman, I. Gouzman, T. K. Minton, L. Shen, A. Stacey, J. Orwa, S. Prawer, B. C. C. Cowie, A. Hoffman, *Diamond Relat. Mater.* **2014**, 45, 20.
- [5] M. Sobaszek, M. Brzezinskaya, A. Olejnik, V. Mortet, M. Alam, M. Sawczak, M. Ficek, M. Gazda, Z. Weiss, R. Bogdanowicz, *Small* **2023**.
- [6] S. Choudhury, R. Golnak, C. Schulz, K. Lieutenant, N. Tranchant, J.-C. Arnault, M.-A. Pinault-Thaury, F. Jomard, P. Knittel, T. Petit, *Carbon* **2021**, 7, 28.
- [7] P. Knittel, F. Buchner, E. Hadzifejzovic, C. Giese, P. Quellmalz, R. Seidel, T. Petit, B. Iliev, T. J. S. Schubert, C. E. Nebel, J. S. Foord, *ChemCatChem* **2020**, 12, 5548.
- [8] M. Mastellone, A. Bellucci, M. Girolami, V. Serpente, R. Polini, S. Orlando, A. Santagata, E. Sani, F. Hitzel, D. M. Trucchi, *Nano Lett.* **2021**, 21, 4477.
- [9] A. F. Sartori, S. Orlando, A. Bellucci, D. M. Trucchi, S. Abrahami, T. Boehme, T. Hantschel, W. Vandervorst, J. G. Buijnsters, *ACS Appl. Mater. Interfaces* **2018**, 10, 43236.
- [10] M. Girolami, A. Bellucci, M. Mastellone, S. Orlando, V. Serpente, V. Valentini, R. Polini, E. Sani, T. De Caro, D. M. Trucchi, *Materials* **2020**, 13, 5761.
- [11] F. Buchner, T. Kirschbaum, A. Venerosy, H. Girard, J.-C. Arnault, B. Kiendl, A. Krueger, K. Larsson, A. Bande, T. Petit, C. Merschjann, *Nanoscale* **2022**, 14, 17188.
- [12] C. Masante, M. Kah, C. Hébert, N. Rouger, J. Pernot, *Dielectr. Mater. Devices, [Proc. Adv. Dielectr. Mater. Multilayer Electron. Devices Symp.]* **2022**, 8.
- [13] A. Chambers, A. Ahnood, S. Falahatdoost, S. Yianni, D. Hoxley, B. C. Johnson, D. J. Garrett, S. Tomljenovic-Hanic, S. Prawer, *Diamond Relat. Mater.* **2020**, 103.
- [14] A. Ahnood, A. N. Simonov, J. S. Laird, M. I. Maturana, K. Ganesan, A. Stacey, M. R. Ibbotson, L. Spiccia, S. Prawer, *Appl Phys Lett* **2016**, 108.
- [15] A. Chambers, S. Prawer, A. Ahnood, H. Zhan, *Front Chem* **2022**, 10.
- [16] S. Falahatdoost, A. Chambers, A. Stacey, H. N. Al Hashem, A. Nadarajah, S. Prawer, A. Ahnood, *Appl. Surf. Sci.* **2021**, 543.
- [17] K. J. P. Quintero, S. Antipov, A. V. Sumant, C. Jing, S. V. Baryshev, *Appl. Phys. Lett.* **2014**, 105.
- [18] P. Calvani, A. Bellucci, M. Girolami, S. Orlando, V. Valentini, R. Polini, D. M. Trucchi, *Carbon* **2016**, 105, 401.
- [19] S. Pezzagna, J. Meijer, *Appl. Phys. Rev.* **2021**, 8.
- [20] J. Raymakers, K. Haenen, W. Maes, *J. Mater. Chem. C* **2019**, 7, 10134.
- [21] N. Yang, S. Yu, J. V. Macpherson, Y. Einaga, H. Zhao, G. Zhao, G. M. Swain, X. Jiang, *Chem. Soc. Rev.* **2018**, 48, 157.
- [22] Z. Jian, N. Yang, M. Vogel, Z. Zhou, G. Zhao, P. Kienitz, A. Schulte, H. Schönherr, T. Jiao, W. Zhang, X. Jiang, *Small Methods* **2020**, 4.
- [23] Y. V. Pleskov, A. Y. S. Akharova, M. D. Krotova, L. L. Bouilov, B. V. Spitsyn, *J. Electroanal. Chem. Interfacial Electrochem.* **1987**, 228, 19.
- [24] K. Patel, K. Hashimoto, A. Fujishima, *J. Photochem. Photobiol., A* **1992**, 65, 419.
- [25] A. Y. Sakharava, Y. V. Pleskov, F. Di Quarto, S. Piazza, C. Sunseri, I. G. Teremetskaya, V. P. Varnin, *J. Electrochem. Soc.* **1995**, 142, 2704.
- [26] L. Boonma, T. Yano, D. A. Tryk, K. Hashimoto, A. Fujishima, *J. Electrochem. Soc.* **1997**, 144, L142.
- [27] Y. V. Pleskov, V. M. Mazin, Y. E. Evstefeeva, V. P. Varnin, I. G. Teremetskaya, V. A. Laptev, *Electrochem. Solid-State Lett.* **2000**, 3, 141.
- [28] F. Maier, J. Ristein, L. Ley, *Phys. Rev. B: Condens. Matter Mater. Phys.* **2001**, 64.
- [29] D. Zhu, L. Zhang, R. E. Ruther, R. J. Hamers, *Nat. Mater.* **2013**, 12, 836.
- [30] L. Zhang, D. Zhu, G. M. Nathanson, R. J. Hamers, *Angew. Chem.* **2014**, 53, 9746.
- [31] B. F. Bachman, D. Zhu, J. Bandy, L. Zhang, R. J. Hamers, *ACS Meas Sci Au* **2021**, 1, 46.
- [32] J. B. Cui, J. Ristein, L. Ley, *Phys. Rev. B* **1999**, 60, 16135.
- [33] T. Petit, M. Lounasvuori, A. Chemin, P. Bärmann, *ACS Meas Sci Au* **2023**.
- [34] T. Petit, H. Yuzawa, M. Nagasaka, R. Yamanoi, E. Osawa, N. Kosugi, E. F. Aziz, *J. Phys. Chem. Lett.* **2015**, 6, 2909.
- [35] T. Petit, M. Pflüger, D. Tolksdorf, J. Xiao, E. F. Aziz, *Nanoscale* **2015**, 7, 2987.
- [36] M. Rusu, T. Kodalle, L. Choubrac, N. Barreau, C. A. Kaufmann, R. Schlattmann, T. Unold, *ACS Appl. Mater. Interfaces* **2021**, 13, 7745.
- [37] D. Thomas, *AIP Adv.* **2022**, 12, 065206.
- [38] T. Dittrich, S. Fengler, *Semicond. Sci. Technol.* **2023**, 38.
- [39] D. S. Ellis, Y. Piekner, D. A. Grave, P. Schnell, A. Rothschild, *Front. Energy Res.* **2022**, 9.
- [40] J. F. Morar, F. J. Himpfel, G. Hollinger, J. L. Jordon, G. Hughes, F. R. McFeely, *Phys. Rev. B* **1986**, 33, 1346.
- [41] J. F. Morar, F. J. Himpfel, G. Hollinger, G. Hughes, J. L. Jordan, *Phys. Rev. Lett.* **1985**, 54, 1960.
- [42] A. Laikhtman, I. Gouzman, A. Hoffman, G. Comtet, L. Hellner, G. Dujardin, *J. App. Phys.* **1999**, 86, 4192.
- [43] S. Choudhury, B. Kiendl, J. Ren, F. Gao, P. Knittel, C. Nebel, A. Venerosy, H. Girard, J. C. Arnault, A. Krueger, K. Larsson, T. Petit, *J. Mater. Chem. A* **2018**, 6, 16645.
- [44] A. Laikhtman, A. Hoffman, *Surface Science Letters* **2003**, 522, L1.
- [45] A. Hoffman, G. Comtet, L. Hellner, G. Dujardin, M. Petracic, *Appl Phys Lett* **1998**, 73, 1152.
- [46] K. C. Prince, R. Richter, M. De Simone, M. Alagia, M. Coreno, *J. Phys. Chem. A* **2003**, 107, 1955.
- [47] H. A. Girard, T. Petit, S. Perruchas, T. Gacoin, C. Gesset, J. C. Arnault, P. Bergonzo, *Phys. Chem. Chem. Phys.* **2011**, 13, 11517.
- [48] K. Bobrov, G. Comtet, G. Dujardin, P. Bergonzo, C. Mer, *Phys. Rev. B: Condens. Matter Mater. Phys.* **2001**, 63.
- [49] L. Diederich, O. M. Kü, P. Aebi, L. Schlapbach, *Surf. Sci.* **1998**, 418, 219.
- [50] D. Takeuchi, H. Kato, G. S. Ri, T. Yamada, P. R. Vinod, D. Hwang, C. E. Nebel, H. Okushi, S. Yamasaki, *Appl Phys Lett* **2005**, 86, 152103.
- [51] D. Takeuchi, M. Riedel, J. Ristein, L. Ley, *Phys. Rev. B: Condens. Matter Mater. Phys.* **2003**, 68.
- [52] J. M. Ballantyne, *Phys. Rev. B: Condens. Matter Mater. Phys.* **1972**, 6, 1436.
- [53] X. Gao, L. Liu, D. Qi, S. Chen, A. T. S. Wee, T. Ouyang, K. P. Loh, X. Yu, H. O. Moser, *J. Phys. Chem. C* **2008**, 112, 2487.
- [54] J. E. Field, *The Properties of Natural and Synthetic Diamond*, Academic Press, **1992**.
- [55] L. Diederich, O. M. Kü, P. Ruffieux, T. Pillo, P. Aebi, L. Schlapbach, *Surf. Sci.* **1998**, 417, 41.
- [56] Y. V. Pleskov, A. Y. S. Akharova, M. D. Krotova, L. L. Bouilov, B. V. Spitsyn, *J. Electroanal. Chem.* **1987**, 228, 19.
- [57] B. Kiendl, A. H. Day, S. Choudhury, F. Buchner, K. Atak, A. Chemin, C. Merschjann, E. Hadzifejzovic, T. Claridge, K. Larsson, A. Venerosy, M. Lounasvuori, N. Zabarska, B. Iliev, T. Schubert, H. Girard, J.-C. Arnault, T. Petit, J. Foord, A. Krueger, (Preprint) ChemRxiv, <https://doi.org/10.26434/chemrxiv-2022-jm92g>, submitted: Dec.
- [58] A. Nefedov, C. Wöll, *Surface Sciences Techniques* **2013**, 51, 277.
- [59] H. Shinotsuka, S. Tanuma, C. J. Powell, D. R. Penn, *Surf. Interface Anal.* **2015**, 47, 871.
- [60] T. Dittrich, S. Fengler, N. Nickel, *Phys. Status Solidi A* **2021**, 218.